Band gaps of diamond under anisotropic stress

Michael P. Surh, Steven G. Louie, and Marvin L. Cohen
Department of Physics, University of California, Berkeley, California 94720
and Materials Sciences Division, Lawrence Berkeley Laboratory, Berkeley, California 94720
(Received 20 June 1991)

Quasiparticle excitation energies are calculated using the *GW* method for diamond under hydrostatic pressures up to 500 GPa and for one tetragonal configuration under an assumed additional stress in the [001] direction. The self-energy operator is approximated with a model for the static screened Coulomb interaction and a plasmon pole approximation for the dynamically screened interaction. The band gaps increase with hydrostatic pressure. In contrast, the minimum gap decreases upon the application of additional [001] stress, with an extrapolated ultimate metallization pressure of 400 GPa, whereas current experimental extrapolations are for a transition at 700–900 GPa. The lower theoretical value is likely due to excessive anisotropy in the model for the applied stress.

INTRODUCTION

The optical properties of diamond under combinations of hydrostatic pressure and uniaxial stress are of practical interest because of the widespread use of diamond-anvil cells (DAC's) for high-pressure experiments. The DAC is often employed in studies of pressure-induced metal-insulator transitions which are observed either by direct transport measurements or by optically probing through the transparent diamond. The introduction of wires into a DAC is a difficult task (currently impractical for pressures above 100 GPa). Thus much of the literature on metallization at such pressures reports measurements of optical reflectivity and absorption.[1–4] These reflectivity results are difficult to interpret, since the index of refraction of diamond is unknown at high stresses.[5]

Changes in the index of refraction are expected at the face of the diamond anvil, since significant variations of the optical properties of diamond under high stress are well known. Bulk diamond itself begins to absorb visible light and to luminesce in the red range at the highest pressures.[6] The observed optical absorption indicates that strong band-gap reductions result from the applied stress in the DAC. Recently, measurements have been made of the minimum band gap of the diamond anvil as a function of pressure in the sample chamber.[7] So far, these observations are limited to the minimum band gaps that govern absorption and luminescence edges. In contrast, *ab initio* calculations can provide information on the entire excitation spectrum and provide estimates of indices of refraction at different points in the DAC.

Early theoretical studies of the band structure of stressed diamond do not provide quantitative information on the band-gap reduction in the DAC. It is known qualitatively that the pressure coefficient for the minimum band gap in diamond is very sensitive to the degree of anisotropy of the stress. The calculated band gaps are all seen to rise as a function of hydrostatic pressure in the local-density approximation (LDA); these theoretical pressure coefficients are in satisfactory agreement with available experiments.[8–10] It is clear from the positive coefficient that hydrostatic pressure is not the cause of the observed band-gap reduction. In contrast, similar LDA calculations indicate that diamond will metallize at a specific uniaxial stress of 400 GPa (Ref. 11) (applied while keeping the transverse lattice constant fixed at the equilibrium value). However, the stress tensor assumed in Ref. 11 is unlikely to describe the situation obtained in practice.

Previous studies are also unable to give quantitative information on the band gaps because of their use of the local-density approximation. Calculations based on the LDA underestimate both the band gaps and metallization pressures of semiconductors.[12–14] The LDA spectrum is also inappropriate for calculating energy-dependent optical properties, since the Kohn-Sham eigenvalues cannot in general be identified as excitation energies. This difficulty can be avoided by using the *GW* approach to calculating the quasiparticle band structure of bulk diamond.[14] A formalism exists for employing the *GW* band structure in a calculation of the optical constants and energy-dependent dielectric properties of diamond in the DAC,[15] but this extension will not be examined here.

In this paper, the one-particle spectrum of cubic diamond ($Fd3m$ symmetry) is first calculated at six pressures both in the LDA and in the *GW* approximation using a model dielectric matrix.[16] The DAC is subjected to anisotropic stress with a greater component normal to the face of the diamond than parallel to it. Accordingly, the band-structure calculation is repeated for tetragonal symmetry $F4_1/adm$ under a combination of hydrostatic pressure and uniaxial stress along the [001] axis. The model stress corresponds to a prediction of the maximum anisotropy in stress within the DAC.[17]

The *GW* calculations require the macroscopic dielectric constants for the density response. These quantities have been obtained using the LDA spectra and wave functions in an Adler-Wiser perturbation approach.[18]

The experimental absorption data are compared to the theoretical *GW* results for the band gaps, with special attention to the range of pressures at which diamond is predicted to metallize. Using the model stress tensor of Ref.

17, a part of the diamond anvil is calculated to metallize for a pressure of 400 GPa in the sample chamber; this differs substantially from the experimentally predicted value of 700–900 GPa.[7] The discrepancy suggests that the assumed strain tensor does not describe the DAC. Accordingly, the tetragonal LDA calculation is repeated for a range of stress anisotropies.

STRESSES IN THE DIAMOND ANVIL

The pressure coefficient of the minimum gap is sensitively dependent on the anisotropy of the lattice strain. It is thus crucial to first identify the lattice structure of the strained diamond anvil. X-ray diffraction is unlikely to give the lattice parameters; the relative transparency of diamond to x rays is already widely used to allow diffraction studies of samples inside the DAC. Additionally, the inhomogeneous strain that is present in the anvil tends to blur diffraction lines. Fortunately, knowledge of the stress distribution is sufficient to determine the lattice structure because total-energy LDA calculations provide reasonable estimates of the stress-strain relations of diamond.[8,9,11] This approach assumes a stress tensor as input to the band-structure calculation, so it must be determined *a priori*.

There are at least three possible methods to obtain the position-dependent stress: calculating the stress and strain tensors with appropriate boundary conditions;[17,20] measuring the Raman mode at the Brillouin-zone center;[21,22] or measuring two or more band gaps from the optical absorption spectrum. The first approach will be used here to define a stress tensor for the bulk band-structure calculation.

A stress tensor appropriate for the interior of a diamond anvil is proposed in Ref. 17; it is estimated indirectly from experimental measurements. The analysis is simplified by assuming a semi-infinite anvil with a flat face and a circularly symmetric distribution of pressure applied to the face. This makes a measurement of the radial variation of the pressure at the surface sufficient to determine the stress at all points. The pressure distribution at the interface is measured by x-ray diffraction of metal gaskets placed between the diamond anvils. Diffraction yields the position-dependent lattice constant of the gasket. The equation of state for the gasket is taken from shock compression data, and the corresponding pressure distribution follows.

Once the pressure at the boundaries is fixed, the internal stress along the central axis of the bulk of the diamond is obtained analytically with the assumption of linearity and the superposition principle.[17] The linearized differential equations governing the inhomogeneous stress and strain suggest that the diamond anvil is subjected to a maximally anisotropic stress of the form[17]

$$\sigma_{ij}=\begin{bmatrix}0.29 & 0 & 0\\ 0 & 0.29 & 0\\ 0 & 0 & 0.89\end{bmatrix}P\ , \tag{1}$$

where P is the applied pressure inside the DAC sample chamber. Equation (1) applies to a small region of the diamond located along the central axis beneath the surface of the anvil. The corresponding lattice strain is particularly simple; the atomic $\hat{z}$ coordinates scale linearly with the lattice compression in that direction. Thus, the space group for [001] stressed diamond is ($F4_1/adm$). (Face-centered tetragonal structures are typically reduced to a smaller body-centered tetragonal cell with the $I4_1/amd$ space group, but face-centered axes are retained to reflect the cubic origins.)

An analytic solution for the stress is subject to certain caveats. The approximate shape and the assumption of linearity both limit the accuracy of the solution. The surface pressure distribution that yields Eq. (1) was measured for a pressure of 335 GPa at the center of the DAC chamber. Equation (1), resulting from a linear calculation, implies that the [001] lattice constant is only 86% that of the [100] and [010] directions, and that the volume of a unit cell decreases by 20% in part of the diamond. The linear approximation, however, assumes small displacements of the material from equilibrium.

Nonlinear effects are expected to reduce the anisotropy of the stress; the large hydrostatic component of the stress in Eq. (1) locally increases the shear modulus.[17] The loss of the superposition principle also implies that the measured distribution of surface pressure will not scale with increased force. Similarly, the degree of anisotropy in the stress and the location of the region of maximum anisotropy will change as a function of applied pressure. These effects are expected to be significant at 335 GPa, given the large lattice contraction estimated above.

Finite-element numerical analyses have been performed for the strain on a cylindrically symmetric model of the DAC in the linear approximation,[19] as well as including nonlinear effects,[20] although the stress tensors were not published along the central axis in the latter case.

Equation (1) serves as an adequate starting point for a calculation. It will be most accurate at the lowest pressures, although the simplified geometry will still introduce some error. Note that it does not include any shear component to the stress; the shear is zero along the cylindrical axis by symmetry. Experimental measurements will inevitably sample regions with some shear stress, so that calculations of the shear dependence of the gap are needed for detailed comparison to experiment.

NUMERICAL PROCEDURE

The GW calculation[14] begins with the LDA eigenfunctions and eigenvalues, which are obtained in this case from a norm-conserving pseudopotential calculation in a plane-wave basis.[23] The carbon pseudopotentials are obtained from a scheme devised by Troullier and Martins[24] that yields excellent potentials for plane-wave-basis calculations. The calculations are done with a cutoff of 50 Ry for the plane-wave basis, so that the gap is converged to the 0.01-eV level.

LDA calculations are performed for bulk diamond at a given lattice constant and a given amount of [001] compression. Stress is then calculated by standard

methods for obtaining forces.[25] The calculated cubic equilibrium lattice constant is $a_0=3.53$ Å with a bulk modulus $B_0=459$ GPa, and $B_0'=4.25$ from a fit to the Murnaghan equation of state for hydrostatic pressure.[26] This is comparable to other theoretical estimates and is in good agreement with the experiment values of 3.567 Å, 443 GPa, and 4, respectively.[8–11] The Young's modulus is estimated to be 1090 GPa, as compared to the other calculated and experimental values of 1050 and 1081 GPa, respectively.[10,11] Poisson's ratio is calculated to be 0.12, as compared to an experimental value of 0.11.[10,11] Accurate stress values require well-converged total energies for the given lattice configuration, so the plane-wave-basis cutoff is increased to 70 Ry.

Polarizability calculations are performed for each lattice configuration to determine the static electronic density response needed for calculating the screened electron-electron interaction. The perturbation formalism is straightforward in terms of the LDA one-particle states.[27] The static-independent particle polarizability χ^0 is obtained in a periodic crystalline potential by an Adler-Wiser scheme,[18]

$$\chi^0_{\mathbf{G}\mathbf{G}'}(\mathbf{q},\omega=0)=\frac{4}{\Omega}\sum_{v,c;\mathbf{k}}\frac{(\langle v\mathbf{k}|e^{-i(\mathbf{q}+\mathbf{G})\cdot\mathbf{r}}|c\mathbf{k}+\mathbf{q}\rangle\langle c\mathbf{k}+\mathbf{q}|e^{i(\mathbf{q}+\mathbf{G}')\cdot\mathbf{r}'}|v\mathbf{k}\rangle)}{\varepsilon_{v\mathbf{k}}-\varepsilon_{c\mathbf{k}+\mathbf{q}}}\ , \tag{2}$$

where $v\mathbf{k}, c\mathbf{k}$ are valence and conduction eigenstates with LDA eigenvalues $\varepsilon_{v\mathbf{k}}, \varepsilon_{c\mathbf{k}}$. Some care must be taken in defining matrix elements for $\mathbf{q}\to 0$, lest some terms incorrectly equal zero (e.g., $\chi_{\mathbf{G}=0,\mathbf{G}'=0}$).[27,28]

The dielectric matrix is given in the random-phase approximation (RPA) by

$$\epsilon^{-1}_{\mathbf{G}\mathbf{G}'}(\mathbf{q},\omega=0)=1+V_C(\mathbf{q})\frac{\chi^0_{\mathbf{G}\mathbf{G}'}(\mathbf{q},\omega=0)}{1-V_C(\mathbf{q})\chi^0_{\mathbf{G}\mathbf{G}'}(\mathbf{q},\omega=0)}\ . \tag{3}$$

All quantities are expressed in a matrix form with indices $\mathbf{G}$ and $\mathbf{G}'$ representing the underlying periodicity of the system. The macroscopic dielectric constant is obtained by inverting the $\mathbf{G}=\mathbf{G}'=0$ element of the inverse dielectric matrix at $\mathbf{q}\to 0$.

The RPA only considers the effects of the self-consistent field due to the direct Coulomb interaction V_C; the effects of exchange and correlation are not included. This RPA expression is appropriate for use in the GW approximation, which neglects the vertex correction.[29]

Once obtained, the macroscopic dielectric constant ϵ_0 is used to define a model static dielectric matrix $\epsilon_{\mathbf{G}\mathbf{G}'}(\mathbf{q})$.[16] This is extended to finite energies by a dielectric band-structure plasmon-pole approximation, and is used to define the dynamically screened Coulomb interaction $W(E)$.[30] The self-energy operator Σ is formed in the GW approximation from W and the one-particle Green function G (Ref. 14)

$$\Sigma(\mathbf{r},\mathbf{r}';E)=\frac{i}{2\pi}\int dE' e^{-i\delta E'}G(\mathbf{r},\mathbf{r}';E-E')W(\mathbf{r},\mathbf{r}';E')\ . \tag{4}$$

Quasiparticle excitation energies are given in rydberg units by

$$E_{n\mathbf{k}}\psi_{n\mathbf{k}}(\mathbf{r})=(-\nabla^2+V_{\text{ion}}+V_H)\psi_{n\mathbf{k}}(\mathbf{r})+\int d^3r'\Sigma(\mathbf{r},\mathbf{r}';E_{n\mathbf{k}})\psi_{n\mathbf{k}}(\mathbf{r}')\ . \tag{5}$$

This many-body treatment yields excellent agreement with photoemission and optical experiments.[14]

It is important to note that the density response to a static external probe is distinct from the response used in the GW calculation. The former is obtained in the LDA (Ref. 31) by including the self-consistent field effects of the electron-electron exchange and correlation in addition to the direct Coulomb term in the denominator of Eq. (3). The additional term is included with the derivative of the exchange-correlation potential

$$\mathbf{K}_{\text{xc}}(\mathbf{r})=\frac{\delta V_{\text{xc}}[\rho(\mathbf{r})]}{\delta\rho(\mathbf{r})} \tag{6}$$

so that

$$\epsilon^{-1}(\mathbf{q},\omega)=1+V_C(\mathbf{q})\frac{\chi^0(\mathbf{q},\omega)}{1-V_C(\mathbf{q})\chi^0(\mathbf{q},\omega)-K_{\text{xc}}\chi^0(\mathbf{q},\omega)} \tag{7}$$

with matrix indices suppressed. K_{xc} is a local quantity, since it is taken in the LDA. The full-density functional version of Eq. (7) should give the correct static response, since this is a ground-state property. In practice, the dielectric constant, ϵ_0, is overestimated by the approximations intrinsic to the LDA.

RESULTS FOR HYDROSTATIC PRESSURE

The RPA dielectric constants are shown in Fig. 1 at seven pressures, decreasing slightly with pressure as a result of the widening band gap. Coincidentally, the calculated RPA dielectric constant at equilibrium volume is in close agreement with the experimental value of 5.5;[10] however, the inclusion of the exchange-correlation contributions would increase the plotted dielectric constants from 3% to 5% at different pressures.

Some of the LDA and GW band gaps are presented for zero pressure in Table I along with the pressure coefficients. The LDA results are in good agreement

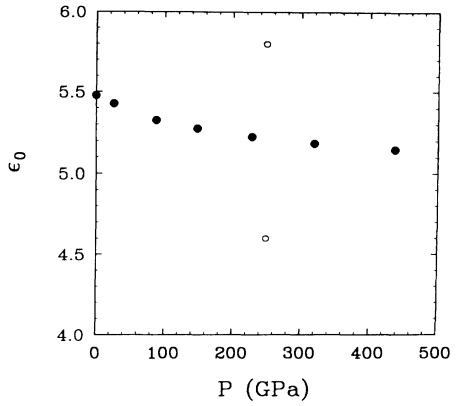

FIG. 1. Dielectric constants ϵ_0 for density response of cubic diamond under hydrostatic pressure and under stress as in Eq. (1) with $P=250$ GPa. RPA results for cubic diamond are represented by solid circles and those for tetragonal diamond by open circles. The tetragonal data point at (250, 5.8) corresponds to taking $\mathbf{q}\rightarrow 0$ along the [100] and [010] directions, while the point at (250, 4.6) corresponds to taking the limit along the [001] direction.

with earlier work.[7,8] Note that the model *GW* approach slightly overestimates most gaps as compared to experiment; the LDA seriously underestimates them. All band gaps are found to increase fairly linearly with pressure and to have a small downward curvature up to pressures as high as 500 GPa. The *GW* method yields larger pressure coefficients than the LDA and is in disagreement with experiment for the coefficient of the fundamental gap. However, any anisotropy in the applied stress will reduce the measured coefficient significantly.

The greater pressure coefficients found in the *GW* approximation are consistent with the behavior in other wide-gap insulators[32] and can be understood to arise from the large changes in the dielectric constant with pressure. The bare exchange contribution to the self-energy is substantially greater for the valence states, which are concentrated in the bonding regions, than for the conduction states. The exchange interaction partly cancels the Coulomb repulsion and therefore lowers the valence band more than the conduction. This band-gap-enhancing effect is reduced, in part, by the effects of screening, so that a decrease in the screening (which occurs in diamond with rising pressure) implies a wider band gap. (For comparison, the Hartree-Fock method neglects screening entirely, and routinely overestimates insulator band gaps.[33])

LDA is based on a jellium electronic system, so it is not surprising that the LDA band gaps do not accurately reflect the influence of changing dielectric properties. The *GW* band gap includes more accurately the effects of the changing screening and thus displays a larger pressure coefficient.

RESULTS FOR HYDROSTATIC PLUS UNIAXIAL STRESS

Some of the band gaps of diamond decrease under the application of uniaxial stress, in contrast to the purely hydrostatic case. The LDA band structures are shown in Fig. 2 for cubic diamond at a volume of 9.02 Å^3 per primitive cell (at a hydrostatic pressure of 126 GPa) and in a tetragonal geometry of the same volume with the [001] axis compressed to 86% of the [100] and [010] axes. The tetragonal case corresponds to a stress of the form of Eq. (1) with $P\simeq 250$ GPa. The minimum gap at this pressure is only 0.56 eV in the LDA (see Table II). Thus, the local-density approximation predicts metallization at a pressure of only 290 GPa inside the sample chamber, given the assumed distribution of stress inside the diamond anvil.

The *GW* calculation requires an input value for ϵ_0; in the tetragonal case, it is dependent on the direction along which $\mathbf{q}\rightarrow 0$. At 250 GPa, the RPA values for the density response are 4.6 for $\mathbf{q}$ in the [001] direction and 5.8 in the [100] and [010] (see Fig. 1). These two limiting values for ϵ_0 are averaged with a 1:2 weighting to be used as input to the *GW* calculation [$\epsilon^{-1}(\mathbf{q}\rightarrow 0)$ is thus isotropic]. The forced isotropy of the long-range screening only affects a few components in the dielectric matrix, and this approximation does not reduce the accuracy of supercell surface *GW* calculations where the RPA screening anisotropy is large.[34] The precise value of the input ϵ_0 is not expected to be critical to the model; varying the input ϵ_0 for silicon by almost 30% changes the 0.6-eV band-gap correction by less than 0.1 eV.[14]

The LDA and *GW* band gaps for tetragonal diamond can be seen in Table II. Band gaps decrease substantially with pressure in both the LDA and *GW*. It is important to note that the precise value of the pressure coefficient depends sensitively on the degree of stress anisotropy in Eq. (1). The pressure coefficient of the minimum band

TABLE I. Band gaps of diamond at zero applied pressure and the corresponding pressure coefficients. All energies are measured in eV from the valence-band maximum; the pressure coefficients are in units of meV/GPa. The experimental values are taken from Ref. 10, data labeled LO-LDA and PW-LDA are local orbital LDA results from Ref. 9 and the plane-wave basis LDA results presented here, respectively. The *GW* results from Ref. 14 for unstressed diamond are 5.6 eV for the fundamental gap and 7.5 for the direct gap; similar results (5.3 and 7.3, respectively) are obtained in Ref. 36.

	Band gaps			Pressure coefficients			
	PW-LDA	*GW*	Expt.	LO-LDA	PW-LDA	*GW*	Expt.
$E_g^{\min}$	4.15	5.68	5.5	5.3	5.7	6.7	5±1
E_g^{dir}	5.57	7.73	7.5	7.0	6.3	7.6	
X_1^c	4.76	6.25		5.1	5.4	6.3	
L_1^c	8.45	10.80		9.6	9.2	10.6	

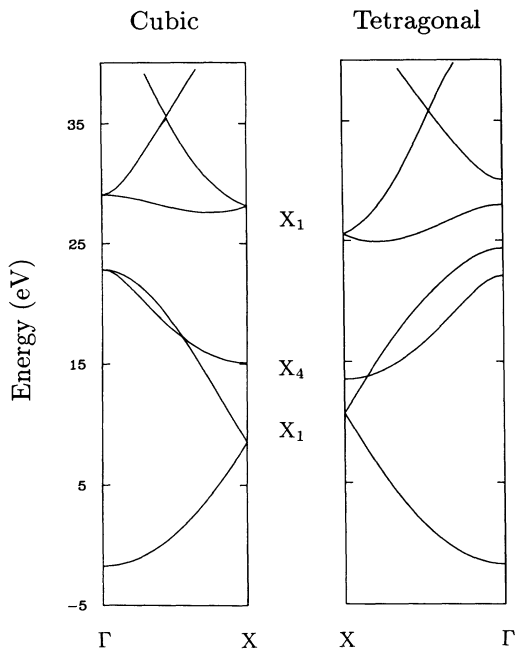

FIG. 2. Band structures of diamond from the Γ to X points (in the [001] direction) for a cubic crystal of volume 9.02 Å^3 per primitive cell corresponding to a hydrostatic pressure of 126 GPa, and for the tetragonal geometry studied [of the same volume, at a pressure given by Eq. (1) with $P=250$ GPa]. Note that the symmetries of the states are unchanged from the cubic case.

gap is estimated to be -14 meV/GPa versus the pressure in the sample chamber, P [see Eq. (1)]. Thus, metallization inside the diamond anvil is expected at pressures of the order of 400 GPa. This disagrees with recent experimental extrapolation for DAC of metallization at 700–900 GPa.[7]

The tetragonal *GW* band gaps could conceivably be in error due to the use of a model dielectric function; however, similar calculations have worked well in surface calculations in a supercell geometry, where the dielectric response is strongly position and direction dependent.[34] The observed equivalence of the LDA and *GW* pressure coefficients is a persistent feature of these calculations. LDA pressure coefficients also tend to agree remarkably well with experiment, except for minor discrepancies such as the slight underestimate of the hydrostatic pressure coefficients here. The *GW* metallization pressure is therefore probably an accurate reflection of what would be induced by the stress tensor given in Eq. (1).

ANALYSIS

The behavior of the band gaps in diamond under hydrostatic pressure has been understood in terms of carbon's position as a first-row element.[9] The low-lying valence and conduction bands are describable by a tight-binding $2s$ and $2p$ Hamiltonian. The atomic orbits of the $n=3$ shell do not enter to lowest order; they act mainly to concentrate bond orbitals along the axes between nearest neighbors.[35] It is sufficient to examine the conduction states at the X point, since the conduction-band minimum lies close by in the Brillouin zone. The lowest-lying valence and conduction states at X are sp hybrids of X_1 symmetry.

Application of hydrostatic stress drives apart the lowest X_1 conduction and valence states and opens the gap. The effect is similar for the nearby conduction-band minimum along Δ. A similar effect is present in group-IV semiconductors, but in Si or Ge the conduction-band minimum is hybridized with a higher-energy-bonding d-orbital state from the same shell as the s and p states. This d-bonding band falls with pressure, so that the hybridized conduction-band minimum also falls in energy. The corresponding d band in diamond derives from the $3d$ atomic orbital and lies too high in energy to participate much. As a result, the behavior of the conduction-band minimum is determined mainly by the tight-binding Hamiltonian for the $2s$ and $2p$ orbitals.

The LDA band structure of tetragonal diamond has been obtained for a crystal at the same volume as for a cubic calculation, for comparison purposes (Fig. 2). The band-gap reduction in the tetragonal case derives from two separate changes in the band structure. First, the tetragonal distortion splits the threefold degenerate, cubic Γ'_{25} valence-band maximum, yielding a singly degenerate valence-band maximum with a doubly degenerate state lying 2.2 eV lower. The zero of the energy scale for the tetragonal case is taken to be the weighted average of the three highest valence bands at Γ, since the symmetry-induced splitting occurs in a 2:1 ratio. The

TABLE II. Band gaps of diamond under hydrostatic pressure $=126$ GPa (cubic); and under anisotropic stress, $P=250$ GPa in Eq. (1) (tetragonal). All energies are measured in eV from the valence-band maximum. Z refers to the X point in the [001] direction; X refers to the [100] and [010] directions. The pressure coefficients are for the tetragonal case in meV/GPa in terms of P in Eq. (1). Note the sensitive dependence on the stress anisotropy of the pressure coefficients as compared to Table I.

	Cubic band energies		Tetragonal band energies		Tetragonal pressure coeff.	
	LDA	*GW*	LDA	*GW*	LDA	*GW*
$E_g^{\min}$	4.77	6.39	0.56	2.07	−14.4	−14.5
E_g^{dir}	6.22	8.52	3.63	5.71	−7.8	−8.1
L_1^c	9.41	11.88	6.46	8.45	−8.0	−9.4
X_1^c	5.31	6.89	5.46	6.96	2.8	2.9
Z_1^c	5.31	6.89	1.17	2.49	−14.4	−15.1

splitting reduces the tetragonal gap by 1.5 eV. Second, the conduction-band minimum along [001] (the direction of stress) decreases in energy (see Fig. 2). (The conduction band at the Γ point also decreases, as a result of the same symmetry-induced splitting that occurs for the valence-band maximum.)

The decrease of the conduction-band minimum is not a result of the reduced symmetry of the tetragonal crystal. The [001] compression does not change the symmetries of the Δ line and X point in the [001] direction, so there is no splitting of degeneracies. Therefore, the movement of the lowest conduction state cannot be explained by new, reduced-symmetry-allowed admixtures with nearby bands. Instead, the behaviors of the X_1-symmetry bands must be understood in terms of changes in specific values of matrix elements of the s and p tight-binding Hamiltonian.

The lowest states of X_1 symmetry (with $\mathbf{k}_X=[001]$) in both the cubic and tetragonal crystals are composed primarily of linear combinations of s and p orbitals of the form

$$\phi=\frac{1}{\sqrt{2}}(S\pm iP_{[001]}) \tag{8}$$

on each atomic site. This is true in the cubic case as well, and similar decompositions with s and p_x,p_y orbitals apply in the tetragonal [100] and [010] directions. These linear combinations of orbitals can be envisioned as ellipsoidal orbitals having a phase that smoothly varies by $\pi/2$ from one end to the other. It is sufficient to examine these tight-binding orbitals on the diamond-lattice basis sites [0,0,0] and $[\frac{1}{4},\frac{1}{4},\frac{1}{4}]a_0$ with phases consistent with $k_X=[001]$ to understand the behavior of the conduction-band minimum. (Note that $k_X=[001]$ and $[00\bar{1}]$ are degenerate, so that only one conduction and one valence band need be considered.)

Phases for the tight-binding wave functions are shown in Figs. 3 and 4 for valence and conduction bands, along with contour plots of the densities for the actual LDA wave functions. The density plots along the inequivalent

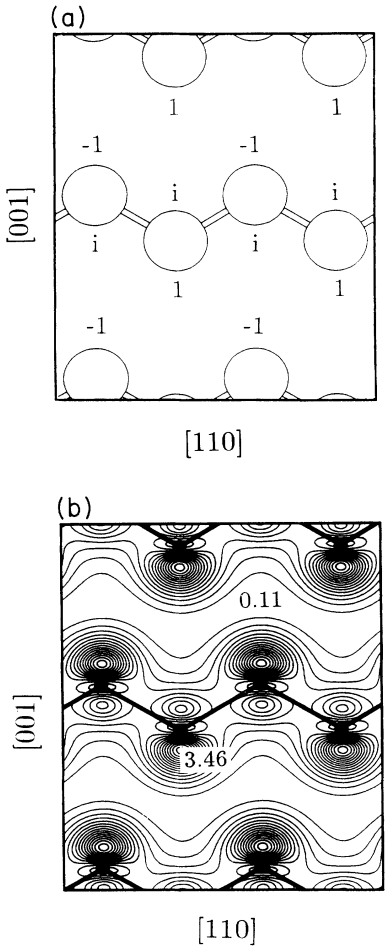

FIG. 3. (a) Ball-and-stick plot of the [110] chain in tetragonal diamond labeling the phases of the tight-binding orbitals of Eq. (8) for an X_1 valence ($\mathbf{k}_X=[001]$) state. Note the equivalent phases all along the center of the [110] chain and opposite phases at the sides of neighboring chains. (b) Charge density (in electrons per primitive cell) of the self-consistent Z_1 valence state in tetragonal diamond. The minima are located between neighboring chains, consistent with the interpretation in the text.

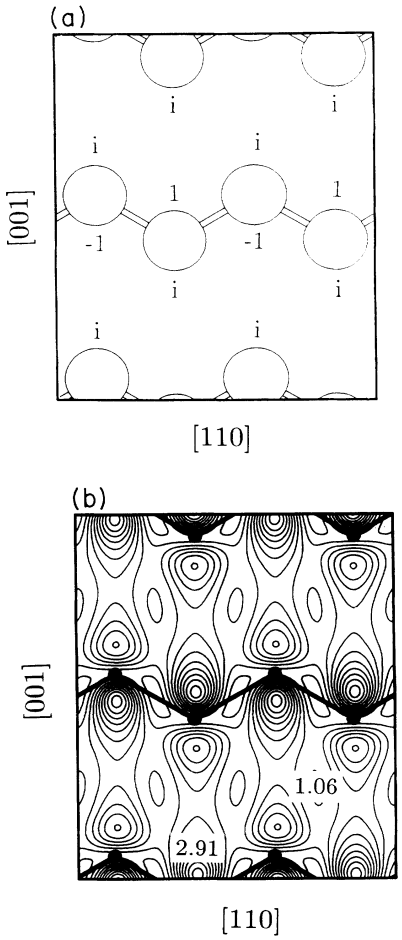

FIG. 4. (a) Ball-and-stick plot of the [110] chain in tetragonal diamond for an X_1 conduction state. The conduction state has alternating signs running along the center of the [110] chain but the same phases on the edges of neighboring chains. (b) Charge density (electrons per primitive cell) of the self-consistent Z_1 conduction state in tetragonal diamond. Minima lie along the center of the [110] chain, consistent with (a) and the text.

[101] ([011], etc.) chains are not shown, as they do not display strain dependences as clearly. It is clear from a bonding-antibonding picture that the valence state can lower its kinetic energy upon compression along the [110] direction, while compression along [001] will raise it [see Figs. 3(a) and 3(b)]. In the latter case the neighboring [110] chains are squeezed together, bringing the nodes of the wave function closer and raising the kinetic energy; in the former case the longitudinal compression of the [110] chains forces them farther apart.

The opposite situation is true for the conduction band [Figs. 4(a) and 4(b)]; hence, the conduction band falls with [001] compression. The X_1 states at [100] and [010] behave in precisely the opposite way (see Table II for numerical data). The behavior under hydrostatic pressure is a combination of these two effects.

The average energy of these X_1 valence and conduction states should be constant, since the splitting is a result of the tight-binding Hamiltonian acting on the degenerate *sp* orbitals. This is, in fact, observed for the two LDA calculations (performed at a fixed unit-cell volume) in Fig. 2 and Table II by comparing the average of the X_1 valence and conduction states to the center of the threefold complex at the valence-band maximum. The differences are constant to within 0.4 eV, despite substantial changes in the detailed band dispersions.

The qualitative behavior of the calculated diamond band gap is thus easily understood, but the quantitative discrepancy with experiment must still be explained. The quoted experimental values are obtained by examining the optical absorption versus energy for light reflected from a solid metal gasket inside the DAC. The optical absorption onset falls with pressure, and the trend is extrapolated to zero gap. Pressures are obtained from the x-ray diffraction lines of the metal gasket. These optical measurements probe the region of smallest band gap. This is probably also the region of maximum anisotropy in the stress. The experiment might be expected to underestimate the metallization pressure, since defect absorption should also contribute. On the other hand, the region of maximum anisotropy is small and therefore contributes relatively little to the total absorption. Reference 17 indicates that the region of maximum anisotropic stress has dimensions on the order of the size of the DAC flat, i.e., 10 μm. This could result in an overestimation of the experimental band gap, particularly since the onset of bulk absorption might be mistaken for defect contributions. Despite the experimental complications, the stress tensor that is assumed for the *GW* calculation is the likeliest source of the discrepancy between experiment and theory.

If the minimum band gap were dependent on only one variable, then the state of stress could be estimated by comparing *GW* calculations to the measured band gaps. However, a decrease in the minimum band gap can arise from one of two changes in the applied stress; either the degree of anisotropy can change while, e.g., leaving the volume fixed, or the ratio between [001], [100], and [010] stresses can be maintained while increasing all three. Thus, the *GW* results for the minimum gap alone cannot be used to deduce the state of stress.

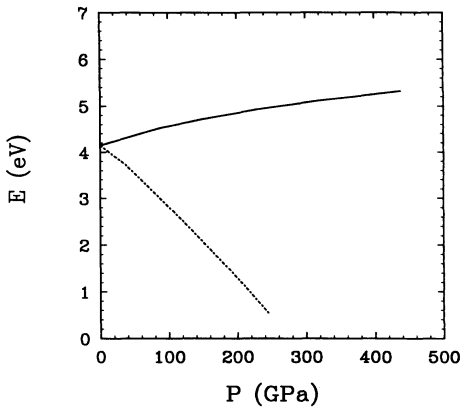

FIG. 5. LDA value for the minimum band gap in eV vs the pressure P for stresses of the form [Eq. (1)]

$$\begin{bmatrix} 0.29 & 0 & 0 \\ 0 & 0.29 & 0 \\ 0 & 0 & 0.89 \end{bmatrix} P$$

for the dotted line, and (hydrostatic)

$$\begin{bmatrix} 1 & 0 & 0 \\ 0 & 1 & 0 \\ 0 & 0 & 1 \end{bmatrix} P$$

for the solid line.

It may be possible to deduce further information by examining other stress-dependent quantities. This has been done in the past with Raman spectra, where the Gruneisen parameter plus the splitting of the threefold degenerate zone center mode can provide enough information to fix the hydrostatic and uniaxial components of the stress state in a small volume.[21]

Similarly, the direct and minimum band gaps depend on the hydrostatic and uniaxial strains in different ways (Figs. 2, 5, and 6). The widening of the band gaps under

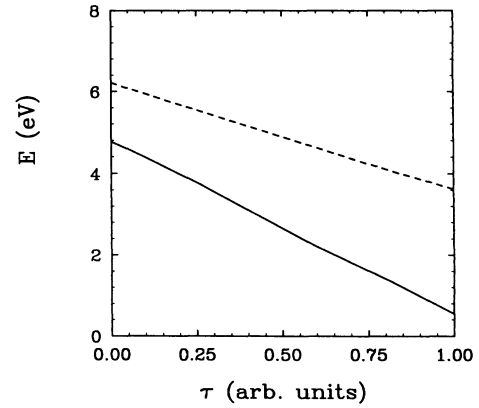

FIG. 6. LDA direct band gap (dashed line) and minimum band gap (solid line) vs the amount of stress anisotropy $\tau=\sigma_{[001]}-\sigma_{[100]}$ obtained while keeping the cell volume fixed. The maximum anisotropy corresponds to the form of Eq. (1), while zero anisotropy corresponds to the hydrostatic pressure required to give the same cell volume.

hydrostatic stress is explained in terms of the splitting of bonding and antibonding sp^3 states.[10] A straightforward, symmetry-induced splitting then lowers the conduction band at Γ upon application of uniaxial stress (Fig. 2). The conduction-band minimum decreases in energy for a different reason, so it has a different dependence on uniaxial stress. This suggests that accurate measurements of the minimum and direct band gaps together can uniquely fix the state of stress by comparison to theoretical calculations.

CONCLUSIONS

The pressure dependence of the diamond direct and minimum gaps has been studied under hydrostatic pressure and hydrostatic pressure plus uniaxial stress. Stresses inside a diamond-anvil cell along the central axis can be described by this two-dimensional parameter space. The effects of shear which is present away from the central axis have not been considered.

All band gaps increase with hydrostatic pressure in both the local-density and *GW* approximations. The LDA is reasonably successful in predicting pressure coefficients as compared to low-pressure experiments and as compared to the *GW* pressure coefficients. In the case of anisotropic stress, the theoretical results for the change in the band gap are not in agreement with the experiment, probably because the assumed stress tensor does not reflect the experimental situation.

The origin of the band-gap changes under hydrostatic pressure is easily understood from a simple *sp* Hamiltonian framework, as well as the dependence on the stress anisotropy. The quantitative discrepancy with experiment is not surprising, given the sensitivity to anisotropy. It is desirable to reconcile these results with experiment by means of a more precise stress-strain calculation. A purely computational approach to this problem offers a particularly easy way to test the optical parameters of a DAC under different conditions. The combination of good estimates of mechanical strain with accurate band-structure calculations would also make the prediction and engineering of diamond-anvil-cell properties possible.

ACKNOWLEDGMENTS

This work was supported by NSF Grant No. DMR88-18404 and the Director, Office of Energy Research, Office of Basic Energy Sciences, Materials Science Division of the U.S. Department of Energy under Contract No. DE-AC03-76SF00098. We particularly wish to thank A. L. Ruoff for providing copies of unpublished work with information on the stress tensor in a DAC and for helpful comments. We would also like to thank G. Martinez and D. Erskine for discussions. One of us (M.P.S.) also wishes to acknowledge Anthony Chen, J. L. Martins, Alberto Garcia, and Xuejun Zhu. CRAY computer time was provided by the NSF at the Pittsburgh Supercomputer Center and the DOE at the National Energy Research Supercomputer Center.

[1]R. Reichlin, M. Ross, S. Martin, and K. Goettel, Phys. Rev. Lett. **56**, 2858 (1986).
[2]R. Reichlin, K. E. Brister, A. K. McMahan, M. Ross, S. Martin, Y. K. Vohra, and A. L. Ruoff, Phys. Rev. Lett. **62**, 669 (1989).
[3]R. J. Hemley and H. K. Mao, Phys. Rev. Lett. **63**, 1393 (1989).
[4]H. K. Mao, R. J. Hemley, and M. Hanfland, Phys. Rev. Lett. **65**, 484 (1990).
[5]J. H. Eggert, F. Moshary, W. J. Evans, H. E. Lorenzana, K. A. Goettel, and I. F. Silvera, Phys. Rev. Lett. **66**, 193 (1991).
[6]P. M. Bell, H. K. Mao, and K. Goettel, Science **226**, 542 (1984); J. A. Xu, H. K. Mao, and P. M. Bell, *ibid.* **232**, 1404 (1986).
[7]A. L. Ruoff, H. Luo, and Y. K. Vohra, J. Appl. Phys. **69**, 6413 (1991).
[8]P. E. Van Camp, V. E. Van Doren, and J. T. Devreese, Phys. Rev. B **34**, 1314 (1986), and experimental references therein.
[9]S. Fahy and S. G. Louie, Phys. Rev. B **36**, 3373 (1987), and experimental references therein; see also S. Fahy, K. J. Chang, S. G. Louie, and M. L. Cohen, *ibid.* **35**, 5856 (1987).
[10]*Numerical Data and Functional Relationships in Science and Technology,* edited by O. Madelung, Landolt-Börnstein, New Series, Vol. 17a (Springer-Verlag, New York, 1982).
[11]O. H. Nielsen, Phys. Rev. B **34**, 5808 (1986).
[12]J. P. Perdew and M. Levy, Phys. Rev. Lett. **51**, 1884 (1983).
[13]L. J. Sham and M. Schlüter, Phys. Rev. Lett. **51**, 1888 (1983).
[14]M. S. Hybertsen and S. G. Louie, in *Proceedings of the 17th International Conference on the Physics of Semiconductors,* edited by D. J. Chadi and W. A. Harrison (Springer-Verlag, New York, 1985), p. 1001; Phys. Rev. Lett. **55**, 1418 (1985); Phys. Rev. B **34**, 5390 (1986).
[15]Z. H. Levine and D. C. Allan, Phys. Rev. Lett. **63**, 1719 (1989).
[16]M. S. Hybertsen and S. G. Louie, Phys. Rev. B **37**, 2733 (1988).
[17]A. L. Ruoff and H. Luo (unpublished).
[18]S. L. Adler, Phys. Rev. **126**, 413 (1962); N. Wiser, *ibid.* **129**, 62 (1963).
[19]D. M. Adams and A. C. Shaw, J. Phys. D **15**, 1609 (1982).
[20]W. C. Moss, J. O. Hallquist, R. Reichlin, K. A. Goettel, and S. Martin, Appl. Phys. Lett. **48**, 1258 (1986); W. C. Moss and K. A. Goettel, *ibid.* **50**, 25 (1987).
[21]M. Hanfland and K. Syassen, J. Appl. Phys. **57**, 2752 (1985).
[22]M. Hanfland, K. Syassen, S. Fahy, S. G. Louie, and M. L. Cohen, Phys. Rev. B **31**, 6896 (1985).
[23]J. Ihm, A. Zunger, and M. L. Cohen, J. Phys. C **12**, 4409 (1979); **13**, 3095(E) (1980).
[24]N. Troullier and J. L. Martins, Solid State Commun. **74**, 613 (1990); Phys. Rev. B **43**, 1993 (1991).
[25]O. H. Nielsen and R. M. Martin, Phys. Rev Lett. **50**, 697 (1983); Phys. Rev. B **32**, 7780 (1985).
[26]F. D. Murnaghan, Proc. Natl. Acad. Sci. U.S.A. **3**, 244 (1944).
[27]M. S. Hybertsen and S. G. Louie, Phys. Rev. B **35**, 5585 (1987); **35**, 5602 (1987).
[28]R. M. Pick, M. H. Cohen, and R. M. Martin, Phys. Rev. B **1**, 910 (1970).
[29]L. Hedin, Phys. Rev. **139**, A796 (1965).
[30]W. von der Linden and P. Horsch, Phys. Rev. B **37**, 8351 (1988).
[31]S. Baroni and R. Resta, Phys. Rev. B **33**, 7017 (1986).
[32]H. Chacham, X. Zhu, and S. G. Louie, Europhys. Lett. **14**, 65

(1991).
[33]R. Dovesi, C. Pisani, F. Ricca, and C. Roetti, Phys. Rev. B **22**, 5936 (1980); W. von der Linden, P. Fulde, and K.-P. Bohnen, *ibid.* **34**, 1063 (1986).
[34]X. Zhu, S. B. Zhang, S. G. Louie, and M. L. Cohen, Phys. Rev. Lett. **63**, 2112 (1989); X. Zhu and S. G. Louie, Phys. Rev. B **43**, 12 146 (1991).
[35]L. Pauling, *The Nature of The Chemical Bond,* 3d ed. (Cornell University Press, Ithaca, NY, 1980), p. 126.
[36]R. W. Godby, M. Schlüter, and L. J. Sham, Phys. Rev. B **37**, 10 159 (1988).